Electronic Supplementary Material (ESI) for Journal of Materials Chemistry A.

Supporting Information

Unraveling cooperative synergy of graphene quantum dots and metal nanocrystals at zero-dimension enabled by layer-by-layer assembly

Zhiping Zeng,[b] Fang-Xing Xiao,[a]* Hung Phan,[c] Shufen Chen,[b] Zhongzhen Yu,[b] Rong Wang,[d] Thuc-Quyen Nguyen,[c] Timothy Thatt Yang Tan [b]*

[a.] College of Materials Science and Engineering, Fuzhou University, Fuzhou 350108, China.

[b.] School of Chemical and Biomedical Engineering, Nanyang Technological University, Singapore 639798, Singapore.

[c.] Center for Polymers and Organic Solids, Department of Chemistry and Biochemistry, University of California, Santa Barbara, CA 93106, United States.

[d.] Singapore Membrane Technology Center, Nanyang Environment and Water Research Institute, Interdisciplinary Graduate School, Nanyang Technological University, Singapore 637141, Singapore.

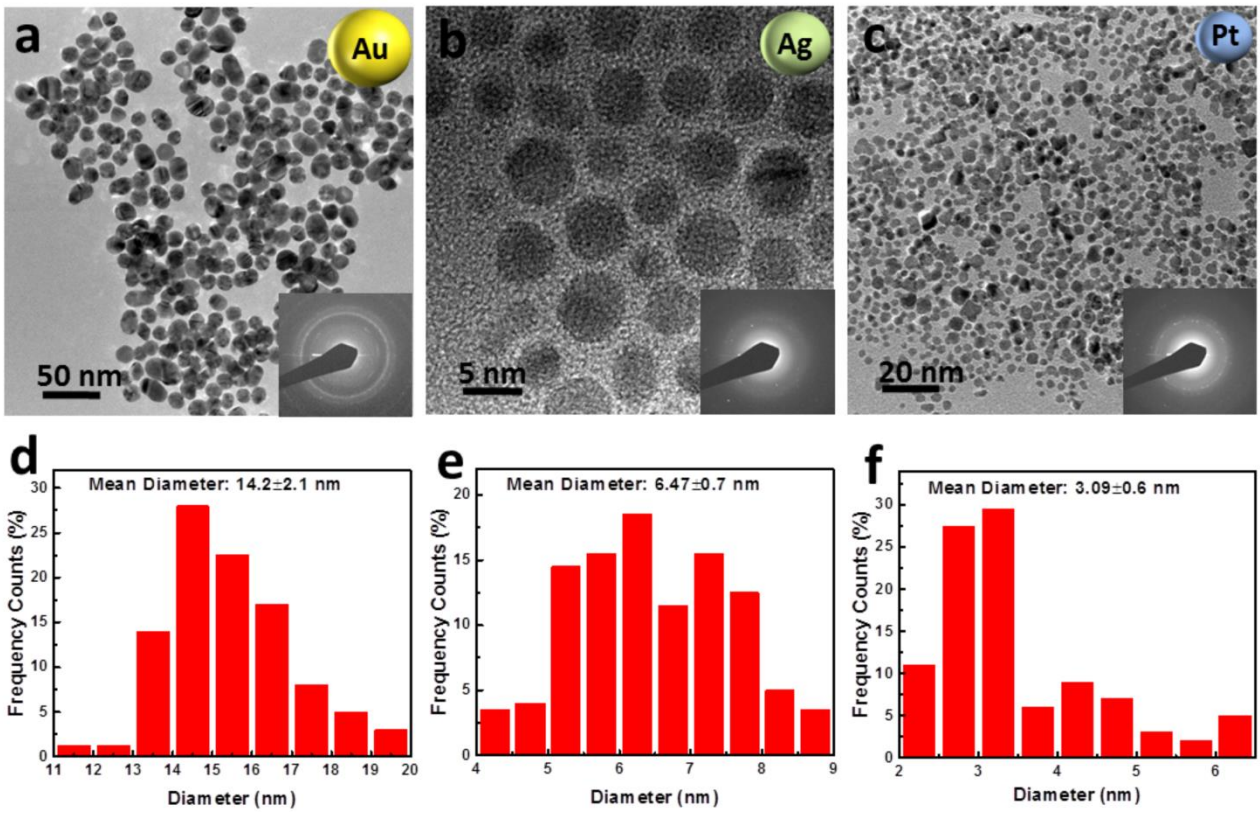

Fig. S1. (a-c) TEM images of citrate-stabilized (a) Au, (b) Ag, and (c) Pt NPs with corresponding SAED patterns in the insets, and (d-f) mean diameter histograms of (d) Au, (e) Ag, and (f) Pt NPs.

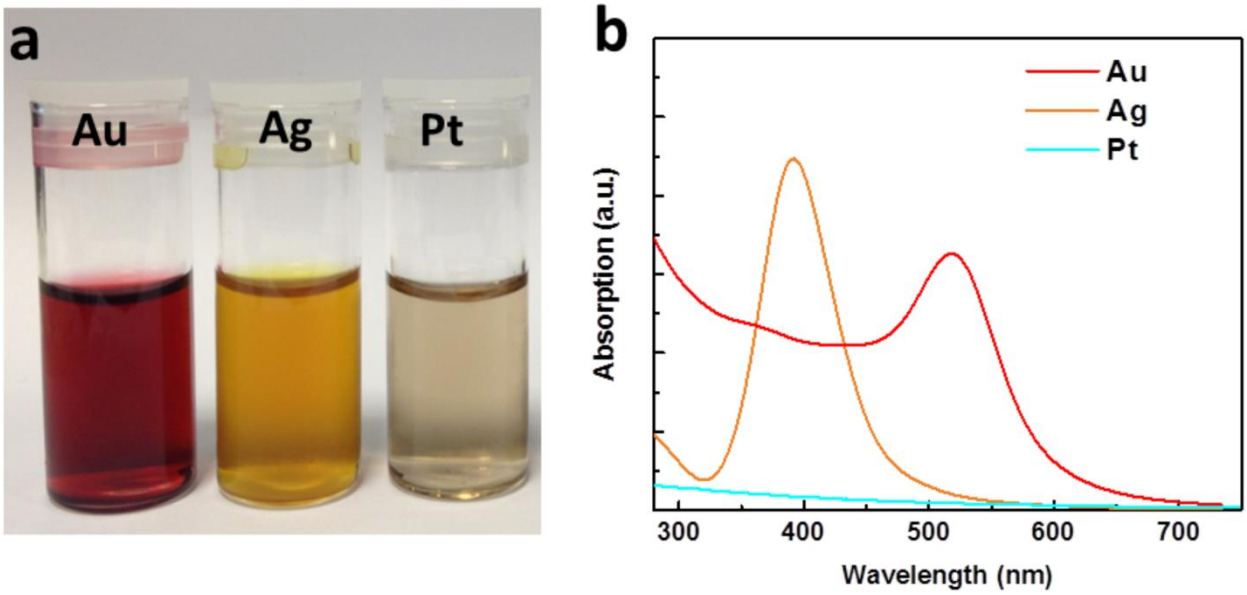

Fig. S2. (a) Photographs and (b) UV-vis absorption spectra of metal NPs aqueous solutions.

Note: It can be observed that UV-vis spectra of metal nanoparticles (NPs) aqueous solutions displayed distinct surface plasmon resonance (SPR) absorption bands at 530 nm for Au and 410 nm for Ag, and no SPR peak was observed for Pt NPs. The results are in agreement with previous results.[1,2]

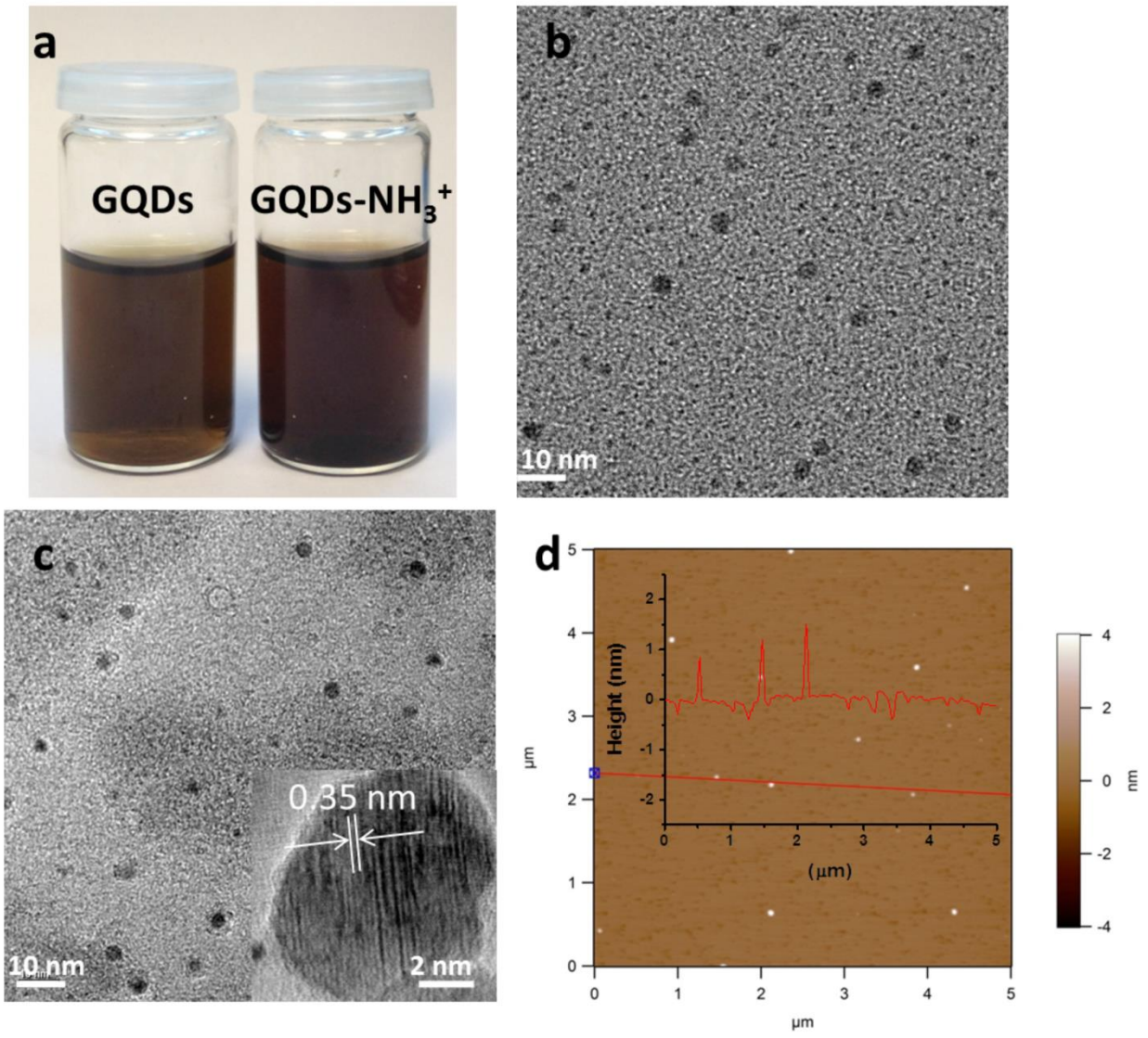

Fig. S3. (a) Photographs of GQDs and GQDs-NH_3^+ aqueous solutions, (b) TEM image of GQDs, (c) TEM image of GQDs-NH_3^+ (Inset: high-resolution image), and (d) AFM image of GQDs-NH_3^+ with corresponding height profile in the inset.

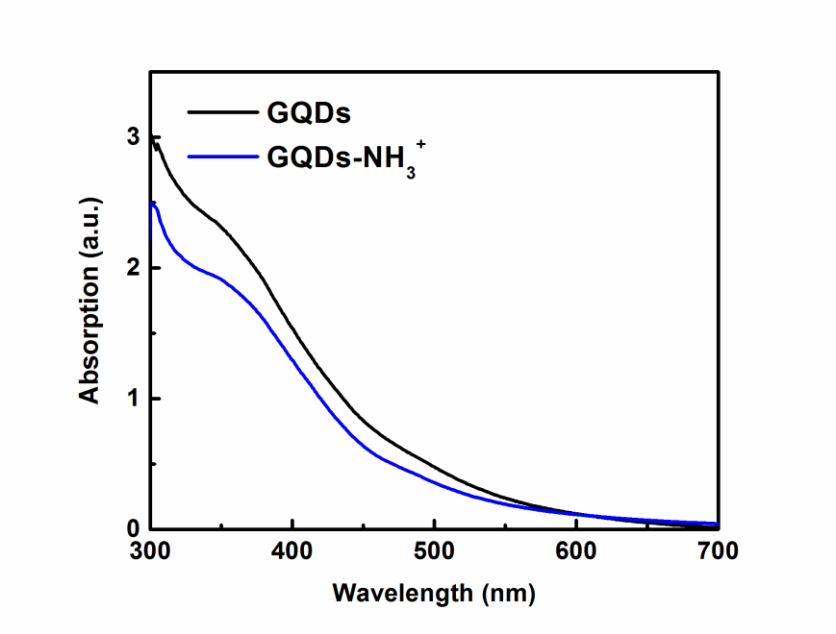

Fig. S4. UV-vis absorption spectra of GQDs and GQDs-NH_3^+ aqueous solutions.

Note: UV-vis absorption spectrum of GQDs-NH_3^+ aqueous solution is similar to that of pure GQDs aqueous solution, for both of which an obvious absorption peak at 355 nm was clearly observed.

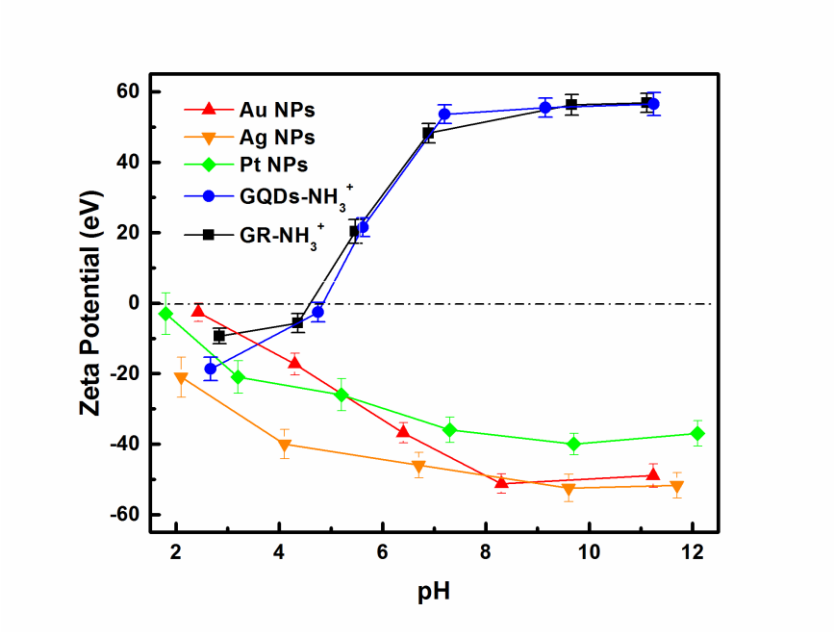

Fig. S5. Zeta potentials of Au, Ag, Pt NPs and GQDs-NH_3^+ as a function of pH value.

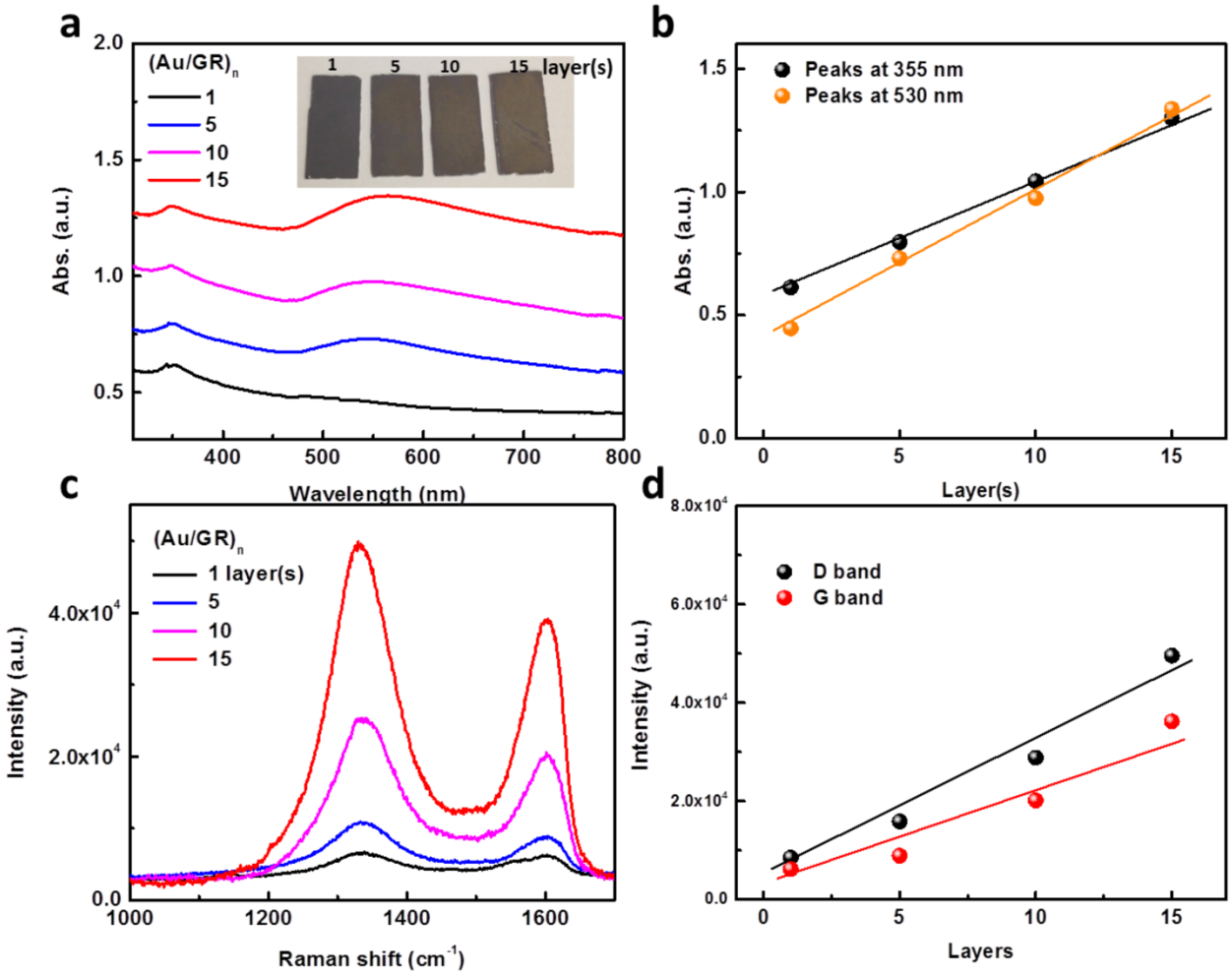

Fig. S6. (a) UV-vis diffuse reflectance spectra (DRS) of $(Au/GR)_n$ (n=1, 5, 10, 15) multilayer films and (b) absorption peak intensity at 355 and 530 nm as a function of the number of assembly cycles. (c) Raman spectra of $(Au/GR)_n$ (n=1, 5, 10, 15) multilayer films and (d) the peak intensity of D and G bands as a function of the number of assembly cycle.

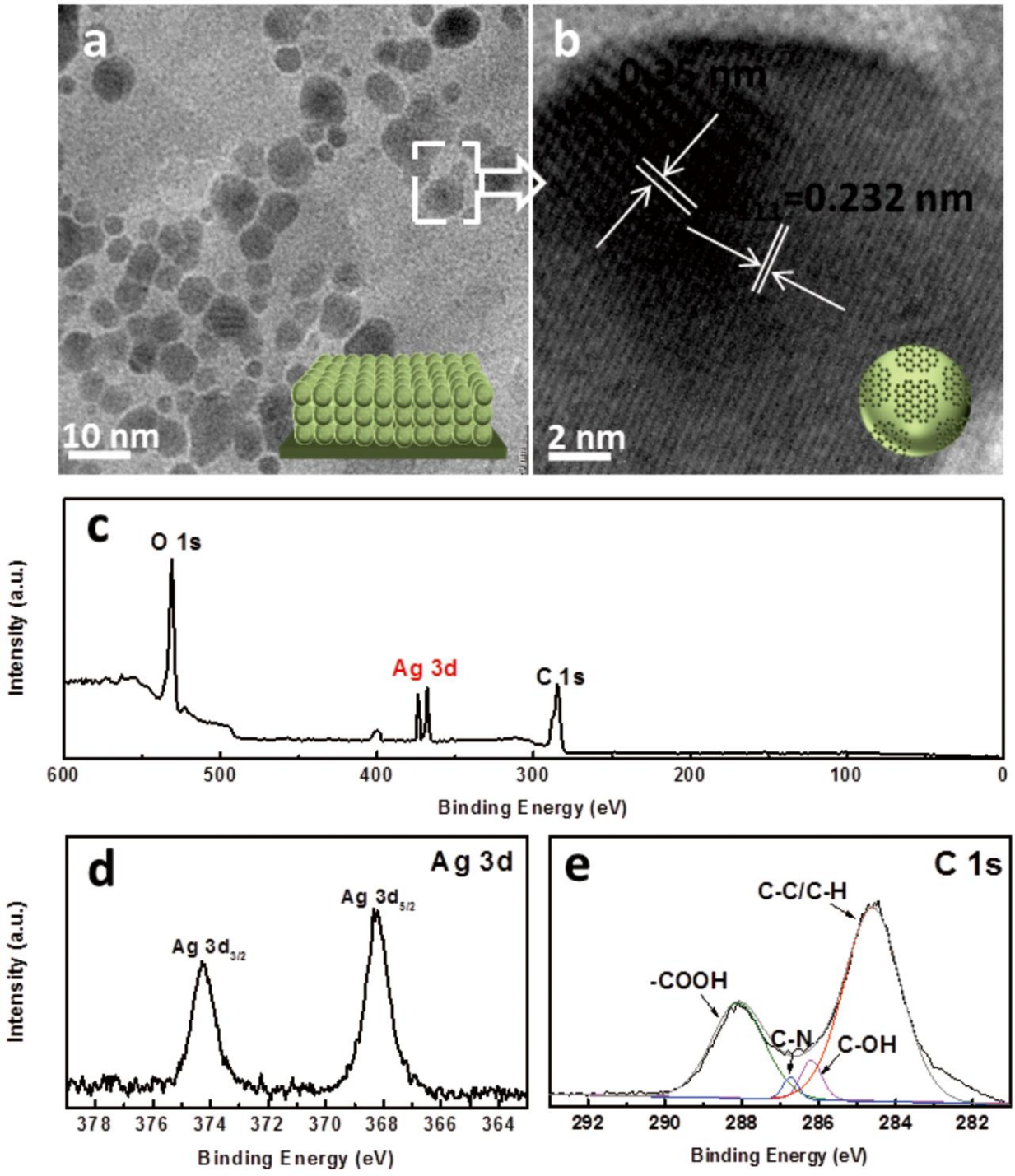

Fig. S7. (a) TEM and (b) HRTEM images of $(Ag/GQDs)_{10}$ films, (c) survey and high-resolution spectra of (d) Ag 3d, and (e) C 1s for $(Ag/GQDs)_{10}$ films.

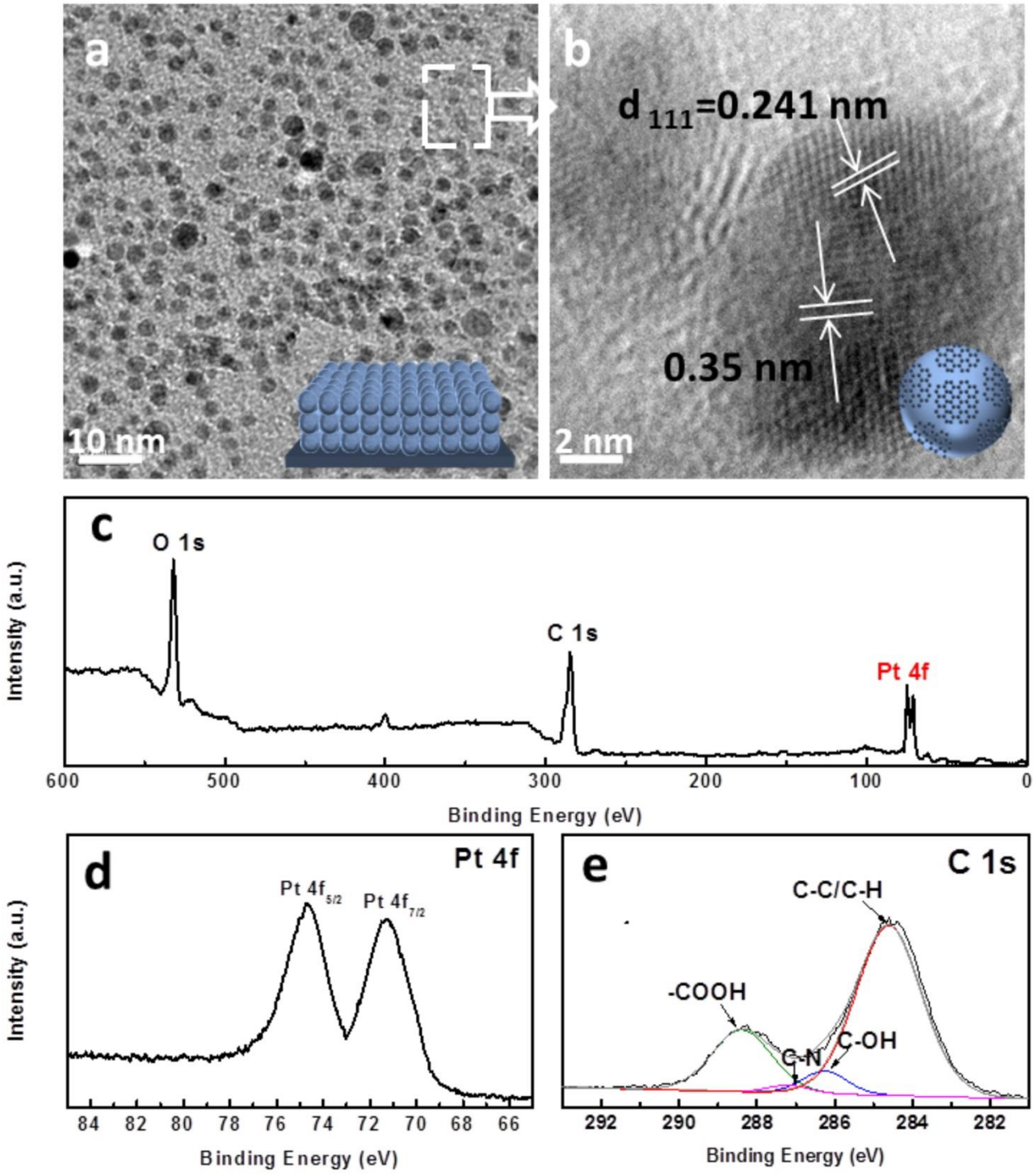

Fig. S8. (a) TEM and (b) HRTEM images, (c) survey and high-resolution spectra of (d) Pt 4f, and (e) C 1s for $(Pt/GQDs)_{10}$ films.

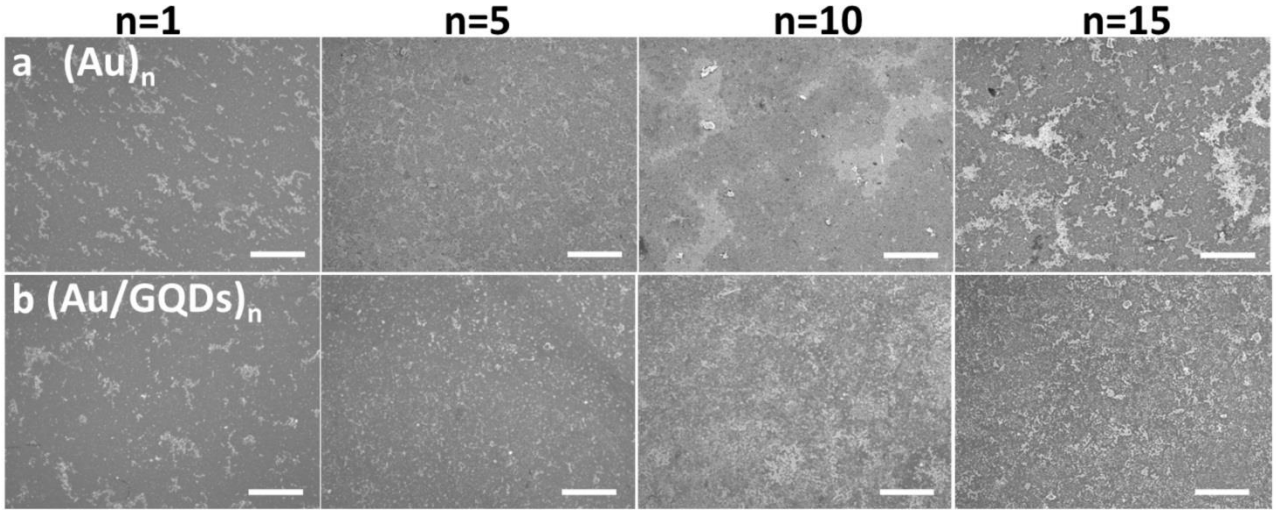

Fig. S9. Top-view FESEM images of (a) $(Au)_n$ and (b) $(Au/GQDs)_n$ (n=1, 5, 10, 15) multilayer thin films, scale bar is 2 μm.

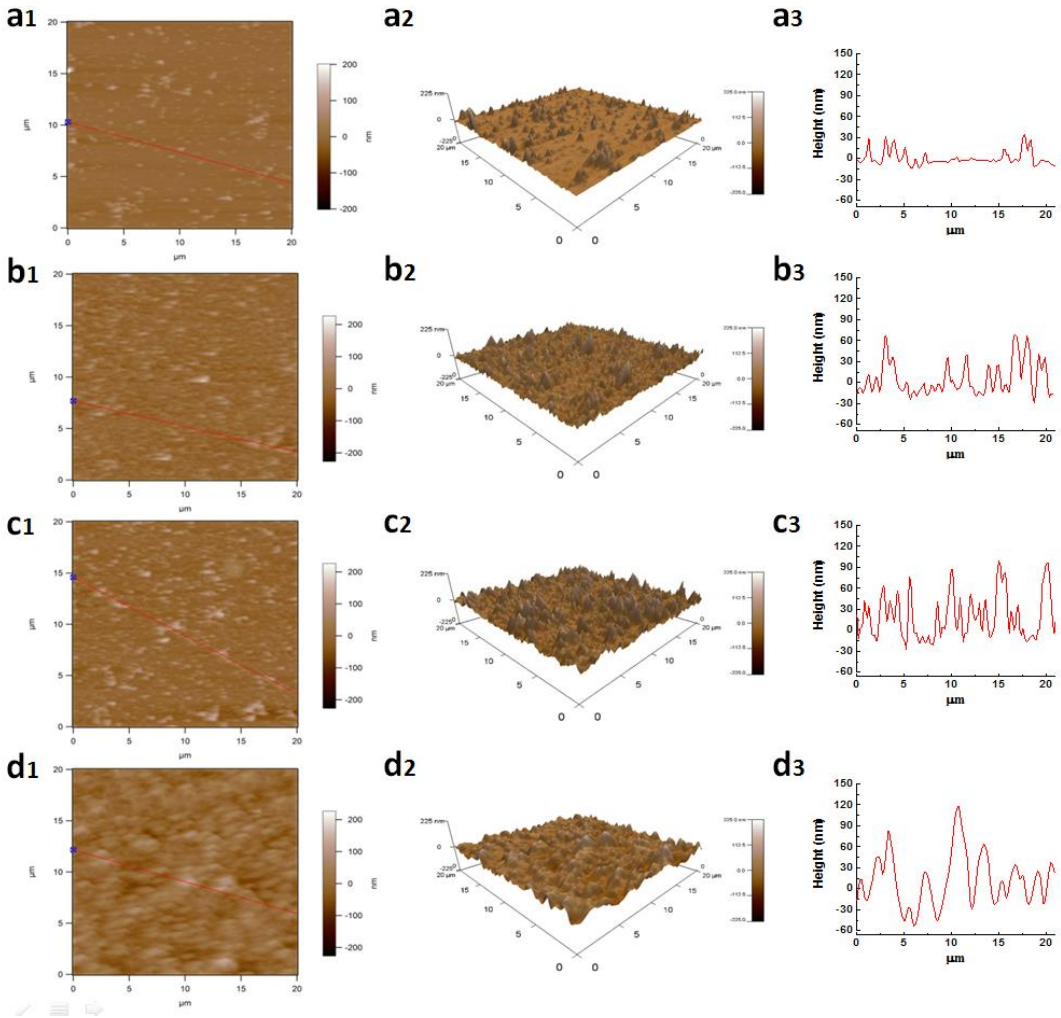

Fig. S10. AFM images of $(Au/GQDs)_n$ multilayer thin films with varying assembly cycle (a) n=1, (b) n=5, (c) n=10, (d) n=15, along with corresponding 3D images and height profiles.

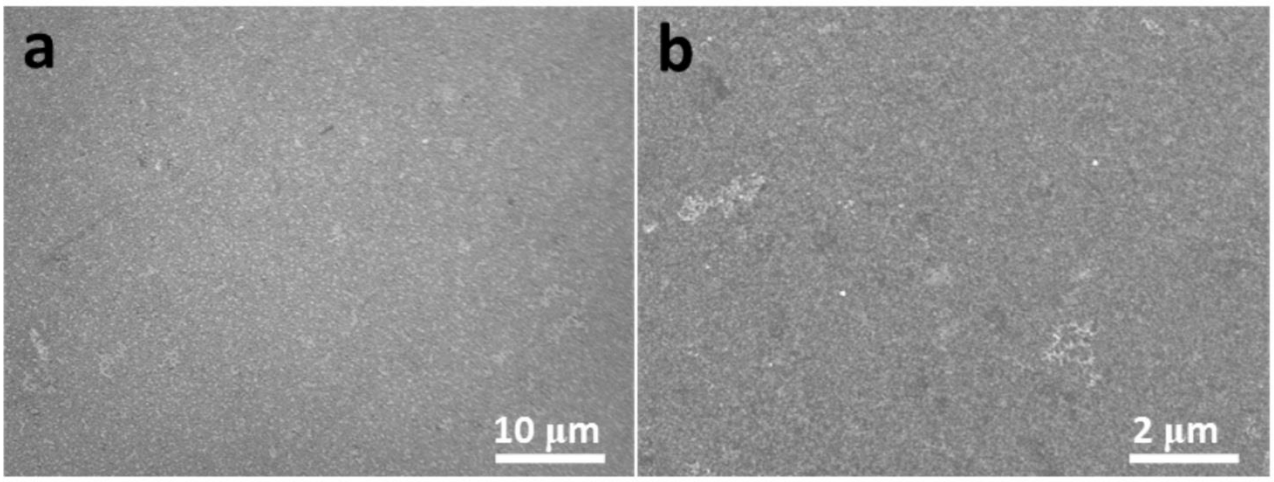

Fig. S11. Panoramic FESEM images of (a) $(Ag/GQDs)_{10}$ and (b) $(Pt/GQDs)_{10}$ multilayer thin films.

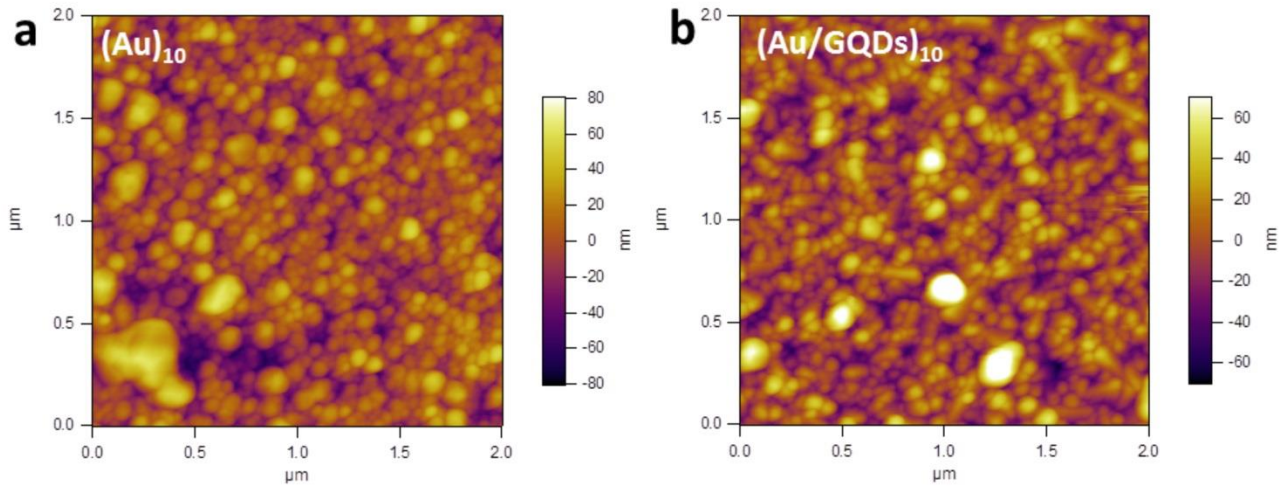

Fig. S12. c-AFM images of (a) $(Au)_{10}$ and (b) $(Au/GQDs)_{10}$ electrodes with a scan size of 2×2 µm and a 10 mV bias potential was applied to the FTO substrate.

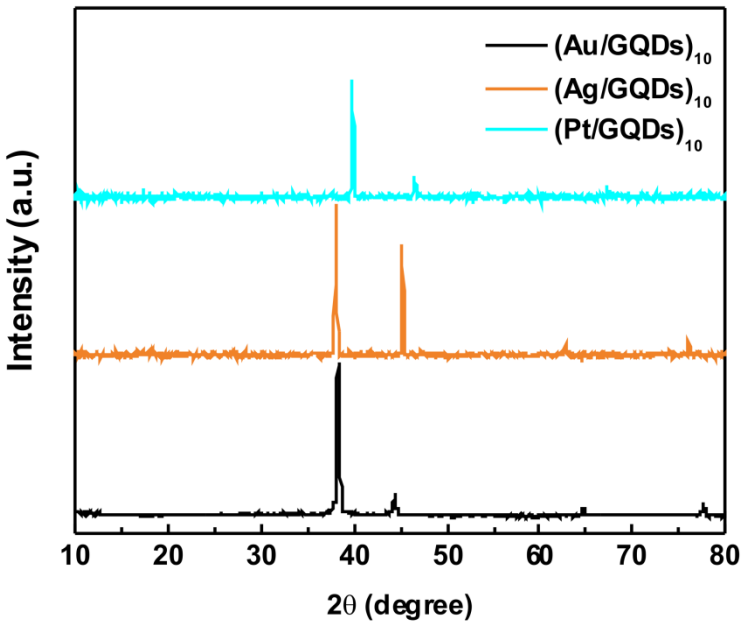

Fig. S13. XRD patterns of $(Au/GQDs)_{10}$, $(Ag/GQDs)_{10}$ and $(Pt/GQDs)_{10}$ multilayer thin films.

Note: As shown in **Fig. S14**, $(M/GQDs)_{10}$ films show the featured crystallographic planes of fcc Au (JCPDS file No. 65-2870), Ag (JCPDS file No. 04-0783), and Pt (JCPDS file No. 65-2868). It is noted that no diffraction peaks of GQDs were observed in the composite films, which can be ascribed to relatively low deposition amount of GQDs or, probably, peak intensity of GQDs was shielded by the substantial diffraction peaks of metal NPs.

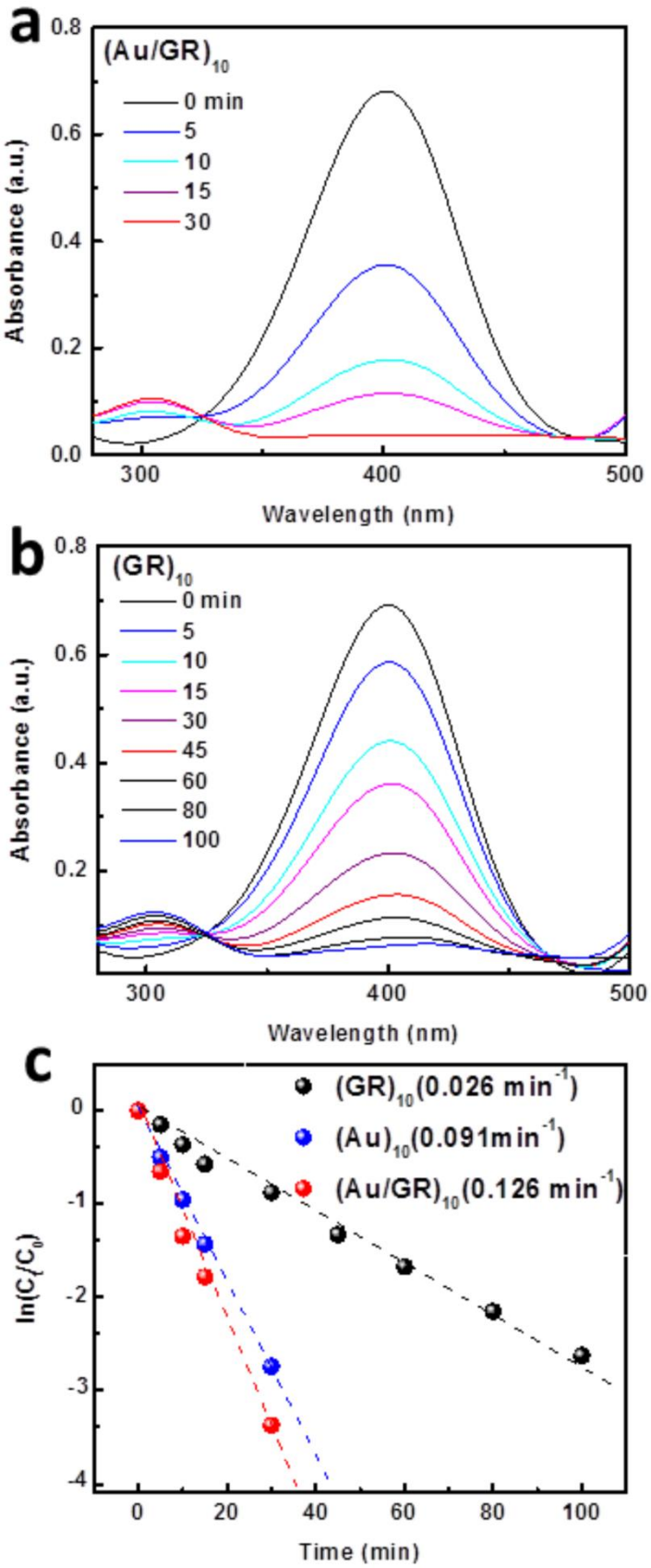

Fig. S14. Time-dependent UV-vis absorption spectra for reduction of 4-NP over (a) $(Au/GR)_{10}$ and (b) $(GR)_{10}$ multilayer thin films. (c) Plots of $\ln(C_t/C_0)$ *vs*. reaction time for reduction of 4-NP over different films.

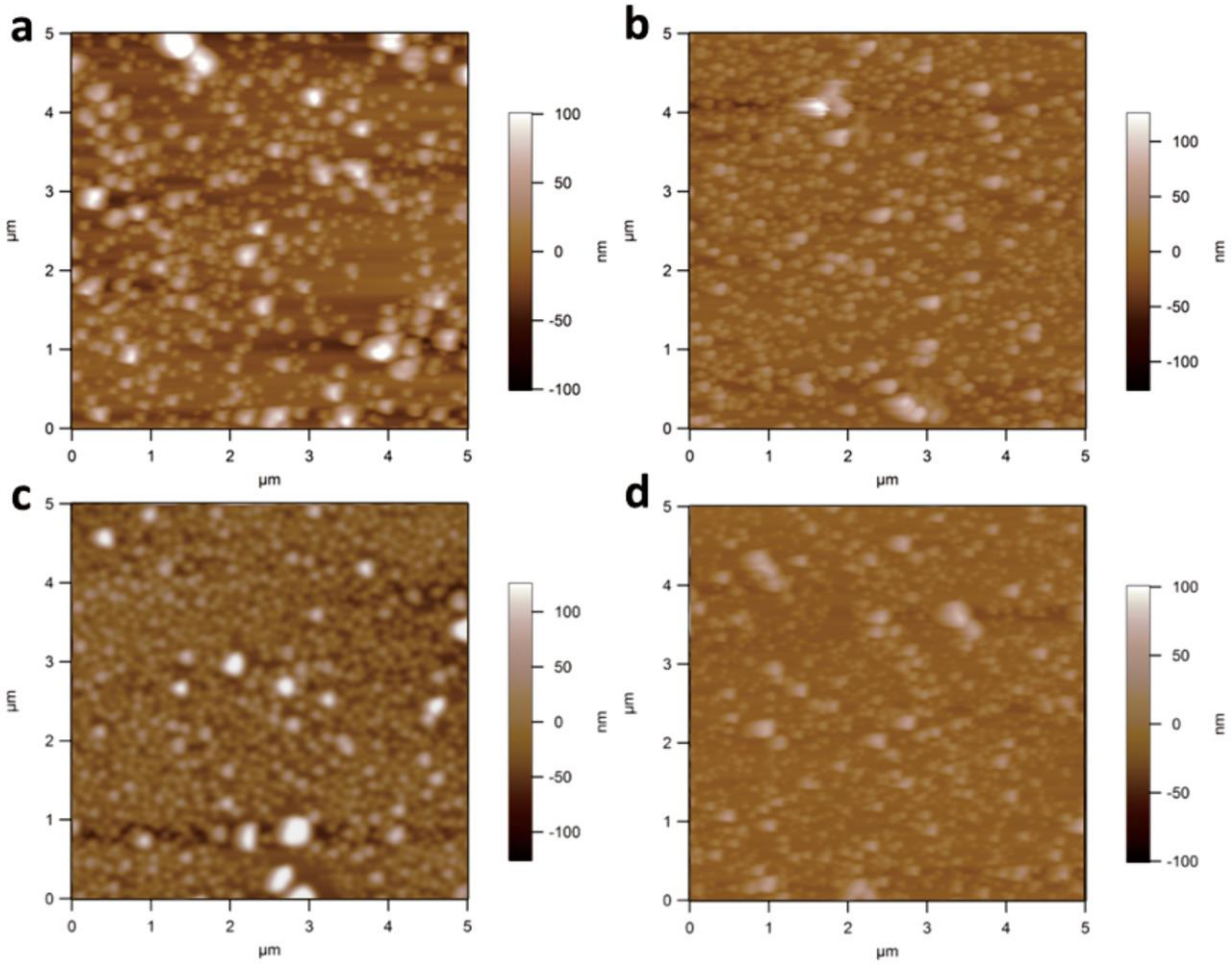

Fig. S15. AFM images of $(Au/GQDs)_{10}$ multilayer films (a) before and (b) after catalytic reactions, , (c) electrocatalytic methanol oxidation, and (d) photoelectrocatalytic reactions.

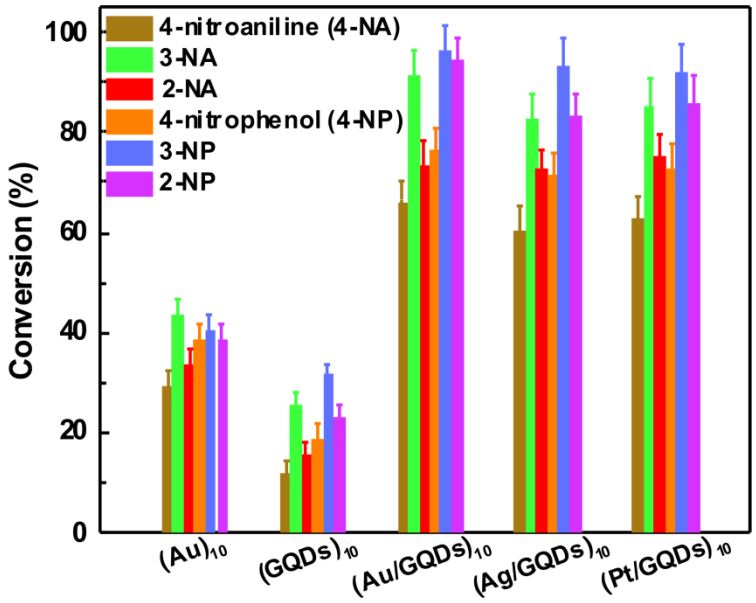

Fig. S16. Selective catalytic reduction of a series of aromatic nitro compounds including 4-NA, 3-NA, 2-NA, 4-NP, 3-NP, and 2-NP over $(Au)_{10}$, $(GQDs)_{10}$, $(Au/GQDs)_{10}$, $(Ag/GQDs)_{10}$, and $(Pt/GQDs)_{10}$ multilayer thin films for the same reaction time (10 min) at ambient conditions.

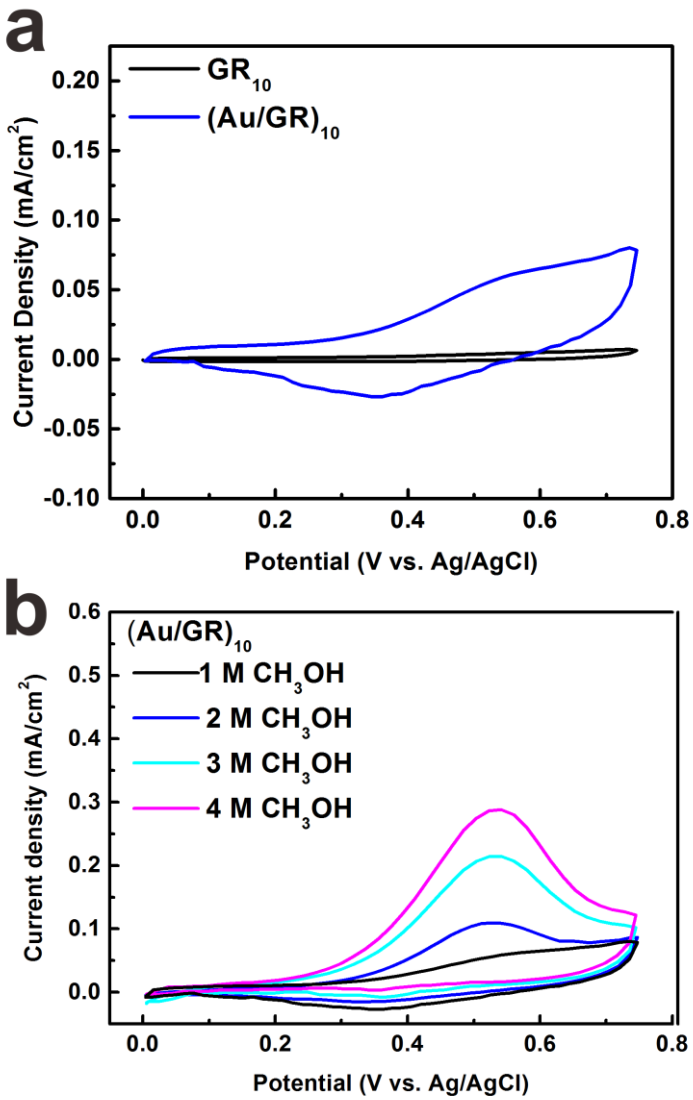

Fig. S17. (a) CV results of $(GR)_{10}$ and $(Au/GR)_{10}$ multilayer films measured in 0.10 M KOH with 1.0 M methanol in a saturated N_2 atmosphere under ambient conditions, and (b) CV results of $(Au/GR)_{10}$ multilayer thin film with different methanol concentration.

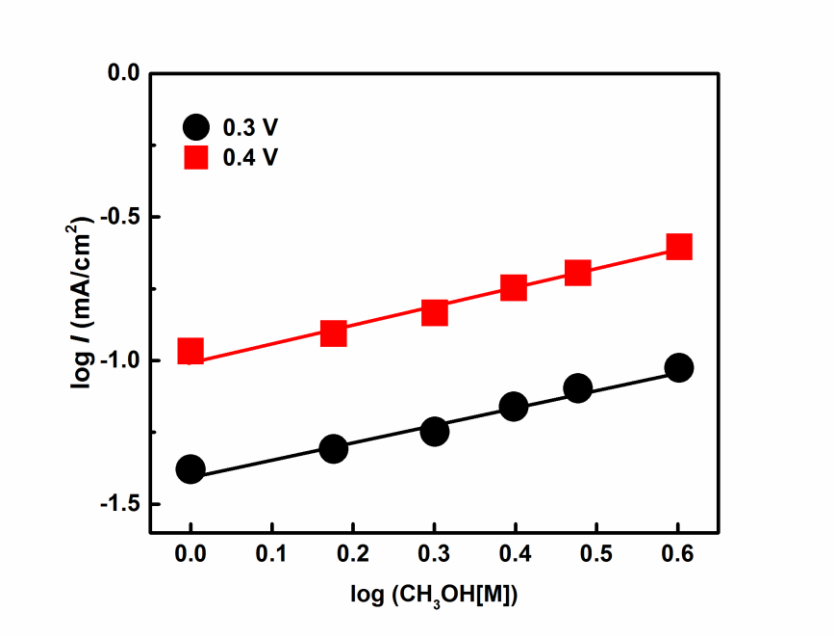

Fig. S18. Plots of log(*I*) against log(C_{CH3OH}) at different potentials in Tafel range.

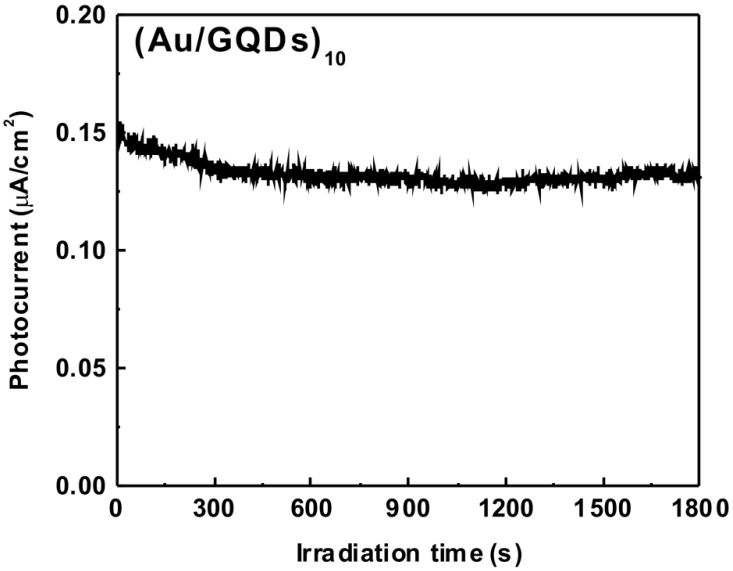

Fig. S19. Photocurrent of $(Au/GQDs)_{10}$ multilayer film under continuous simulated solar light irradiation.

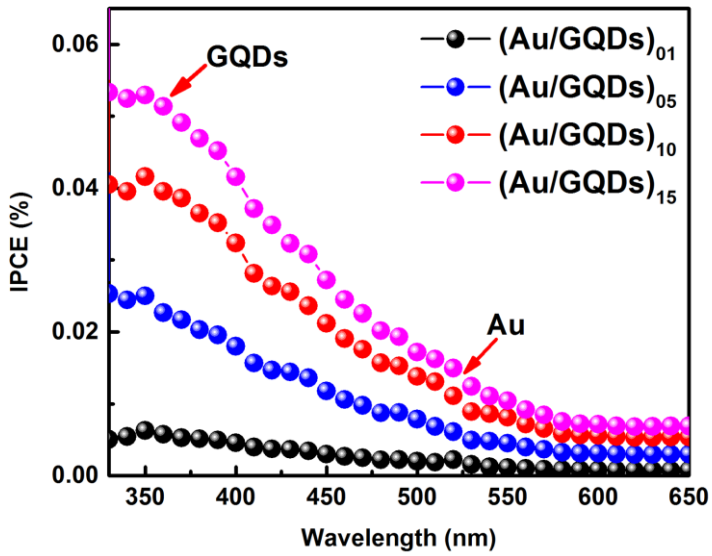

Fig. S20. IPCE spectra of $(Au/GQDs)_n$ (n=1,5,10,15) multilayer thin films.

Table S1. Catalytic reaction rate constants of different multilayer thin films toward reduction of aromatic nitro compounds at ambient conditions.

Sample	4-NA	3-NA	2-NA	4-NP	3-NP	2-NP
$(Au)_{10}$	0.091	0.103	0.097	0.102	0.118	0.109
$(GQDs)_{10}$	0.030	0.038	0.034	0.041	0.051	0.043
$(Au/GQDs)_{10}$	0.345	0.406	0.354	0.398	0.417	0.403
$(Ag/GQDs)_{10}$	0.201	0.346	0.312	0.304	0.386	0.355
$(Pt/GQDs)_{10}$	0.289	0.353	0.337	0.307	0.369	0.363
$(Au/GR)_{10}$	0.126	0.144	0.132	0.139	0.131	0.127

Unit: min^{-1}

Experimental Section

1 Preparation of positively charged graphene oxide quantum dots (GQDs)

a. Preparation of GQDs

Graphene oxide quantum dots (GQDs) were prepared with CX-72 carbon black via being refluxed in a concentrated nitric acid (HNO_3) solution.[3,4] Typically, 0.4 g of dried CX-72 carbon black was added to 6 mol L^{-1} nitric acid (100 mL) and refluxed for 24 h at 110. After cooling to below 30 ℃, the product was centrifuged (12000 rpm) for 10 min to achieve sediment and a supernatant. The resultant supernatant was treated at 200 ℃ to evaporate the nitric acid and water. After cooling to room temperature, a reddish-brown solid was acquired. Finally, GQDs aqueous solution was obtained by dissolving GQDs in DI H_2O under 10 min sonication.

b. Preparation of surface charge-modified GQDs

Positively charged GQDs (GQDs-NH_3^+) or GR aqueous solution was prepared *via* the

1-[3-(dimethylamino)propyl]-3-ethylcarbodiimide methyliodide (EDC) and ethylenediamine (EDC)-mediated amine exchange reaction.[5] To be specific, 0.5 g of EDC was dissolved in 4 mL of ethylenediamine, and the mixture was added into 40 mL of negatively charged GQDs aqueous solution (0.5 mg/mL). The mixed solution was rapidly stirred for 12 h at ambient conditions, and then dialyzed for 3 days in a membrane tube (MWCO = 12000-14000 Da) to remove any residual chemicals after reaction.

2 Synthesis of negatively charged citrate-stabilized metal nanocrystals

a. Preparation of Au NPs

Citrate-stabilized gold nanocrystals (NPs) were prepared by Dotzauer method.[6] Briefly, all glassware was cleaned thoroughly with aqua region (HCl/HNO_3=3:1) and rinsed with DI water. 50 mL of aqueous 1mM $HAuCl_4 \cdot 3H_2O$ was heated to a rolling boil with stirring. 5 mL of 38.8 mM sodium citrate dihydrate was also heated to a rolling boil and then added rapidly to the gold solution. After 20 s, the mixture became dark and then burgundy, and was subsequently heated with stirring for 10 min and stirred without heating for an additional 15 min.

b. Preparation of Ag NPs

Citrate-stabilized silver NPs were prepared according to Lee's approach.[7] Briefly, 100 mL of 1 mM aqueous $AgNO_3$ solution was mixed with 8 mL of a 40 mM aqueous sodium citrate solution used as stabilizer. 2 mL of 112 mM aqueous $NaBH_4$ solution was then added dropwise under vigorous stirring at ambient temperature, immediately yielding a yellowish brown Ag hydrosol. The Ag hydrosol was subsequently stocked in a refrigerator at 4 ℃ and aged for 24 h to decompose the residual $NaBH_4$ before it was used in subsequent steps.

c. Preparation of Pt NPs

Citrate-stabilized platinum NPs was prepared by Elliott's method.[8] Specifically, 26 mL of 2.8 mM aqueous trisodium citrate dehydrate solution was added to 50 mL of 0.4 mM aqueous hydrogen hexachloro-platinate solution at room temperature. An amount of 5 mL of 12 mM $NaBH_4$ was then introduced dropwise with vigorous stirring, and the pale yellow solution turned dark brown in 5 min. Finally, the dark brown colloidal solution was stirred for 4 h and stored in a refrigerator at 4 ℃ for further use.

3 LbL assembly of $(M/GQDs)_n$ (M=Au, Ag, Pt) multilayer thin films

Fluorine-doped tin oxide (FTO) or silicon wafer substrates were thoroughly cleaned in a freshly prepared "piranha" solution (3:1 concentrated 98% H_2SO_4/30% H_2O_2; Caution: piranha solution reacts violently with organic materials and should be handled with great care). Firstly, the substrate was dipped into polyethylenimine (PEI) aqueous solution (1.0 mg/mL, 0.5 M NaCl, pH=7.2) for 10 min and washed three times with DI H_2O, followed by drying with a gentle stream of N_2. Subsequently, the resultant substrate was immersed in as-prepared negatively charged metal aqueous solution for 10 min and then subjected to the same washing and drying treatments. Afterward, the substrate was dipped into surface charge modified GQDs (or GR) aqueous suspension (1.0 mg/mL, pH=7.0) for 10 min, rinsed with DI H_2O, and dried by a stream of N_2, thus producing $(M/GQDs)_1$ or $(M/GR)_1$ multilayer thin film. The above procedure as a whole was designated as one assembly cycle. Multilayer $(M/GQDs)_n$ or $(M/GR)_n$ composite thin films with varying assembly cycles were prepared by alternate deposition of positively charged GQDs (GR) and negatively charged metal NPs. For comparison, pure $(GQDs)_n$, $(GR)_n$, $(metal\ NPs)_n$, multilayer thin films were also prepared. For the preparation of pure $(GQDs)_n$ (or $(GR)_n$) multilayer thin films, the substrate was dipped into poly (sodium 4-styrenesulfonate) (PSS, 1.0 mg/mL, pH=7.0) aqueous

solution for 10 min and washed three times with DI H_2O, followed by drying with a gentle stream of N_2. Subsequently, the resultant substrate was immersed in surface charge modified GQDs (or GR) aqueous solution for 10 min and then subjected to the same washing and drying treatments, producing $(GQDs)_1$ (or $(GR)_1$) multilayer thin film. Multilayer $(GQDs)_n$ (or $(GR)_n$) thin films with varying assembly cycles were prepared by alternate deposition of negatively charged PSS and positively charged GQDs (or GR). Multilayer (metal $NPs)_n$ thin films with varying assembly cycles were prepared by alternate deposition of positively charged PEI and negatively charged metal NPs. Finally, LbL-assembled multilayer thin films were calcined in an argon atmosphere at 200 ^oC for 1 h at a heating rate of 5 ^oC/min. The detailed assembly procedure was illustrated in **Scheme. 1**. The multilayer films grown on the Si wafer or FTO substrate were first immersed into an ethanol solution and ultra-sonicated for 5 min, by which the samples were gradually peeled off. The obtained ethanol solution was dipped on the copper mesh, and then the copper mesh was dried for TEM measurement.

4 Characterizations

Scanning electron microscopy (SEM) images were acquired with field emission scanning electron microscopy (JEOL, JSM-6700F). Transmission electron microscopy (TEM) and high-resolution transmission electron microscopy (HRTEM) images were achieved by using a JEOL model JEM2010 EX instrument at an accelerating voltage of 200 kV. X-ray photo electron spectroscopy (XPS) measurements were collected through ESCALAB 250 photoelectron spectrometer (Thermo Fisher Scientific) at 2.4×10^{-10} mbar. Binding energy (BE) of the element was calibrated to the BE of carbon (284.60 eV). Atomic force microscopy (AFM) and c-AFM images were obtained by using MFP3D microscope, Asylum Research.[9] UV-vis spectra were recorded on a Shimadzu UV2501

spectrophotometer in which $BaSO_4$ was used a background ranging from 300 to 800 nm. The fluorescence spectra were collected by a Fluoromax-4, Horiba Jobin Yvon Spectro fluorometer with a photon-counting detection system to detect fluorescence emission. Sample excitation was obtained by using a diode laser, BWF-2 (980 nm, P_{max} = 1.0 W at 3.0 A, B &W TEK Inc.) with an optical fiber (100 μm, core). Fourier Transform Infrared Spectroscopy (FTIR) was conducted in a Digilab FTS 3100 instrument by collecting 45 scans with a resolution of 4 cm^{-1}. The crystal phase of the samples was recorded by X-ray diffraction (XRD, Bruker D8 Advance X-ray diffract meter) with Cu Kα radiation. The zeta potential of samples was measured by dynamic light scattering analysis (Zeta PALS, Brookhaven Instruments Co.). Raman results were collected by using Raman spectroscopy (Renishaw) equipped with a 633 nm laser source.

5 Selective catalytic reduction of aromatic nitro compounds

As a representative example, catalytic properties of $(M/GQDs)_n$ (M=Au, Ag, Pt; n=1, 5, 10, 15) multilayer thin films were evaluated by employing the reduction of aromatic nitro compounds to corresponding amino compounds by $NaBH_4$ as a model reaction. In a typical reaction, $(M/GQDs)_n$ samples (20 mm×10 mm) with an area of 2 cm^2 was dipped into an aqueous solution in a quartz cuvette containing 2 mM (40 μL) aromatic nitro compound, 100 mM (400 μL) $NaBH_4$, and 2 mL DI H_2O. Afterward, the mixture was stirred at room temperature for 30 min to generate uniform aqueous solution. The use of a high excess of $NaBH_4$ ensure that its concentration remains essentially constant during the whole reaction, which allows the assumption of pseudo-first-order kinetics with respect to the nitro compounds. Samples of the reaction mixture were collected at a specific time interval for UV-vis spectroscopy analysis.

6 Electrochemical methanol oxidation

Electrochemical experiments were carried out in a three-electrode quartz cell with electrochemical workstation (CHI 66D) in which platinum sheet was employed as counter electrode and Ag/AgCl electrode as reference electrode, and $(M/GQDs)_n$ multilayer thin films with an active area of 15.9 mm^2, provided by a mask with a diameter of 4.5 mm, were used as the working electrodes. Cyclic voltammetry (CV) and linear sweep voltammetry (LSV) were performed between 0.00 to 0.75 V in a 0.1 M KOH solution with or without 1.0 M methanol solution at room temperature at a scan rate of 20 mV/s. Electrochemical impedance spectroscopy (EIS) measurements were performed in the frequency range from 100 kHz to 100 mHz under AC stimulus of 10 mV in amplitude.

7 Photoelectrochemical (PEC) Measurement

PEC measurements were carried out on an electrochemical workstation (Zennium, Zahner). The electrochemical setup is composed of conventional three-electrodes, a quartz cell containing 20 mL Na_2SO_4 (0.5 M) aqueous solution and a potentiostat. A phatinum plate (20 mm × 10 mm) was used as counter electrode and Ag/AgCl as reference electrode. The samples film (20 mm × 10 mm) were vertically dipped into electrolyte and irradiated with a 300 W xenon arc lamp (Newport) equipped with an AM 1.5 filter. Monochromatic incident photo-to-electron conversion efficiency (IPCE) spectra were collected using three-electrode without bias, for which monochromatic light was provided by a 300 W xenon arc lamp (Newport) combined with a monochromator (Newport).

References

1 V. T. P. Vinod, P. Saravanan, B. Sreedhar, D. K. Devi and R. B. Sashidhar, *Colloid Surface B.,* 2011, **83**, 291-298.

2 F. -X. Xiao, *J. Phys. Chem. C,* 2012, **116**, 16487-16498.

3 Z. Zeng, F. -X. Xiao, X. Gui, R. Wang, B. Liu and T. T. Y. Tan, *J. Mater. Chem. A,* 2016, **4**,

16383-16393.
4 Z. Zeng, D. Yu, Z. He, J. Liu, F. -X. Xiao, Y. Zhang, R. Wang, D. Bhattacharyya and T. T. Y. Tan, *Sci. Rep.,* 2016, **6***,* 20142.
5 J. Hong, N. J. Shah, A. C. Drake, P. C. DeMuth, J. B. Lee, J. Z. Chen and P. T. Hammond, *ACS Nano,* 2012, **6**, 81-88.
6 D. M. Dotzauer, J. H. Dai, L. Sun and M. L. Bruening, *Nano Lett.,* 2006, **6**, 2268-2272.
7 J. Yang, J. Y. Lee and H. P. Too, *J. Phys. Chem. B,* 2005, **109**, 19208-19212.
8 C. J. Jiang, J. M. Elliott, D. J. Cardin and S. C. Tsang, *Langmuir,* 2009, **25**, 534-541.
9 Z. He, H. Phan, J. Liu, T. Q. Nguyen and T. T. Y. Tan, *Adv. Mater.,* 2013, **25**, 6900-6904.